Received: 7 May 2020 | Revised: 23 September 2020 | Accepted: 14 October 2020

DOI: 10.1111/nan.12669

Neuropathology and Applied Neurobiology WILEY

ORIGINAL ARTICLE

Linking epigenetic signature and metabolic phenotype in *IDH* mutant and *IDH* wildtype diffuse glioma

Yannick Braun[1] | Katharina Filipski[1,2,3] | Simon Bernatz[1] | Peter Baumgarten[1,4] | Bastian Roller[1] | Jenny Zinke[1] | Pia S. Zeiner[1,5] | Elena Ilina[1] | Christian Senft[4] | Michael W. Ronellenfitsch[2,3,5,6] | Karl H. Plate[1,2,3,6] | Oliver Bähr[5] | Elke Hattingen[6,7] | Joachim P. Steinbach[2,3,5,6] | Michel Mittelbronn[1,8,9,10,11] | Patrick N. Harter[1,2,3,6]

[1]Neurological Institute (Edinger Institute), University Hospital, Goethe University Frankfurt am Main, Frankfurt, Germany

[2]German Cancer Consortium (DKTK) partner site Frankfurt/Mainz, Frankfurt, Germany

[3]German Cancer Research Centre (DKFZ), Heidelberg, Germany

[4]Department of Neurosurgery, University Hospital, Goethe University Frankfurt am Main, Frankfurt, Germany

[5]Dr. Senckenberg Institute for Neurooncology, University Hospital, Goethe University Frankfurt am Main, Frankfurt, Germany

[6]Frankfurt Cancer Institute (FCI), Frankfurt, Germany

[7]Department of Neuroradiology, University Hospital, Goethe University Frankfurt am Main, Frankfurt, Germany

[8]Luxembourg Centre of Neuropathology (LCNP), Luxembourg

[9]Luxembourg Centre for Systems Biomedicine (LCSB), University of Luxembourg, Luxembourg

[10]National Centre of Pathology (NCP), Laboratoire national de santé (LNS), Luxembourg

[11]Department of Oncology (DONC), Luxembourg Institute of Health (LIH), Luxembourg

Correspondence
Patrick N. Harter, Neurological Institute (EdingerInstitute), University Hospital, Goethe University Frankfurt am Main, Frankfurt, Germany.
Email: patrick.harter@kgu.de

Abstract

Aims: Changes in metabolism are known to contribute to tumour phenotypes. If and how metabolic alterations in brain tumours contribute to patient outcome is still poorly understood. Epigenetics impact metabolism and mitochondrial function. The aim of this study is a characterisation of metabolic features in molecular subgroups of isocitrate dehydrogenase mutant (*IDH*mut) and isocitrate dehydrogenase wildtype (*IDH*wt) gliomas.

Methods: We employed DNA methylation pattern analyses with a special focus on metabolic genes, large-scale metabolism panel immunohistochemistry (IHC), qPCR-based determination of mitochondrial DNA copy number and immune cell content using IHC and deconvolution of DNA methylation data. We analysed molecularly characterised gliomas (n = 57) for in depth DNA methylation, a cohort of primary and recurrent gliomas (n = 22) for mitochondrial copy number and validated these results in a large glioma cohort (n = 293). Finally, we investigated the potential of metabolic markers in Bevacizumab (Bev)-treated gliomas (n = 29).

Results: DNA methylation patterns of metabolic genes successfully distinguished the molecular subtypes of *IDH*mut and *IDH*wt gliomas. Promoter methylation of lactate dehydrogenase A negatively correlated with protein expression and was associated with *IDH*mut gliomas. Mitochondrial DNA copy number was increased in *IDH*mut tumours and did not change in recurrent tumours. Hierarchical clustering based on metabolism panel IHC revealed distinct subclasses of *IDH*mut and *IDH*wt gliomas with an impact on patient outcome. Further quantification of these markers allowed for the prediction of survival under anti-angiogenic therapy.

Conclusion: A mitochondrial signature was associated with increased survival in all analyses, which could indicate tumour subgroups with specific metabolic vulnerabilities.

KEYWORDS
glioma, metabolism, mitochondria, DNA methylation, *IDH* mutation

1 | INTRODUCTION

Diffuse gliomas include isocitrate dehydrogenase mutant (*IDH*mut) astrocytic and oligodendroglial tumours, as well as *IDH*mut and *IDH* wildtype (*IDH*wt) glioblastoma (GB). These tumours account for over 60% of primary brain tumours in the adult population in the United States [1]. The combined incidence is 4.2 per 100.000 capita. The 5-year survival rates range from 81.3% for oligodendroglioma to 29.8% for anaplastic astrocytoma and 5.5% for GB [1,2]. Initially, these gliomas were defined only by histology. Molecular alterations, such as *IDH* mutational status and co-deletions of chromosomal arms 1p and 19q can predict patient prognosis [3–5]. Both *IDH*mut and *IDH*wt gliomas are characterised by their diffuse infiltrative behaviour. However, these tumours display distinct epigenetic, genetic and transcriptional characteristics, which result in different outcomes in patients [4,6–9].

IDH mutations result in the conversion of ketoglutarate (KG) to D-2-hydroxyglutarate (D2HG), which inhibits KG-dependent dioxygenases, such as ten-eleven translocation (TET) enzymes as well as Jumonji C domain-containing histone-lysine demethylases [10–13]. This leads to DNA and histone hypermethylation, which ultimately produces a hypermethylation phenotype known as the 'glioma CpG-island methylator phenotype' (G-CIMP) [14,15]. Differences in DNAmethylation patterns allow for artificial intelligence-assisted tumour classification [16]. *IDH*wt GB has been further subdivided into three molecular subgroups: proneural (PN), classical (CL) and mesenchymal (MES). Initially, these subgroups were defined according to distinct gene expression profiling. In addition, DNA methylation analyses enable subdivision into these subgroups [16,17]. In the context of DNA methylation analyses, the subgroups are referred to as RTK I (PN), RTK II (CL) and mesenchymal.

Current treatment standards of *IDH*mut and *IDH*wt gliomas are similar. These treatments rely on tumour resection and combined radiochemotherapy with temozolomide or other DNA alkylating agents [18,19].Trials of targeted therapeutic approaches have produced disappointing results [20–24].

Metabolic reprogramming is a characteristic hallmark of cancer [25]. Normalisation of deregulated cellular energy metabolism in tumours has been hypothesised to be a beneficial factor [25,26]. Pharmacological therapy either directly (e.g. ketogenic diet) or indirectly (e.g. anti-angiogenic treatment) targets cellular energy homoeostasis [27–29]. Anti-angiogenic therapy in GB induces an adaptation towards anaerobic metabolism and induces a hypoxic microenvironment [29,30]. In an *IDH*wt GB patient-derived xenograft model, anti-angiogenic therapy also led to reduced mitochondrial biomass in tumour cells [31].

Metabolic changes in malignant tumours compared to non-neoplastic tissues were first described almost 100 years ago by the German biologist Otto Warburg [32]. He discovered that tumour cells metabolised glucose to lactate via glycolysis despite the presence of oxygen. This phenomenon of aerobic glycolysis is termed the Warburg effect [33,34]. Alterations in glucose metabolism and mitochondrial respiration in cancer have been intensively studied over recent decades. Their contribution to malignant transformation or progression across different cancer entities is undisputed. However, the extent to which metabolic alterations are necessary to sustain the malignant phenotype and the stage of tumour progression at which they occur are unclear. Examining these mechanisms will help to understand the unsuccessful therapeutic attempts of metabolic normalisation in gliomas.

To gain further insights into metabolic regulation of gliomas, we investigated the DNA methylome profiles of *IDH*mut and *IDH*wt gliomas focussing on glucose metabolism and mitochondrial respiration. Additionally, to assess mitochondrial biomass, we analysed mitochondrial DNA copy number profiles. We validated these results using an immunohistochemistry (IHC)-based metabolism panel of three glioma patient cohorts, including patients who had undergone anti-angiogenic treatment. To investigate the influence of the immune microenvironment on our results, we analysed the immune cell content and composition by epigenetic data deconvolution and IHC. The findings revealed that DNA methylation patterns of key metabolic genes are strongly associated with molecular subgroups of gliomas and that *IDH*mut gliomas are enriched for a respiratory mitochondrial signature. A mitochondrial signature in *IDH*wt glioblastomas was also associated with improved patient survival. Finally, patients with a relatively increased mitochondrial signature displayed an improved response to anti-angiogenic treatment.

2 | MATERIALS AND METHODS

2.1 | Patient material and patient cohorts

DNA methylation analyses were performed using samples from 57 patients with glial brain tumours. All samples were collected as formalin-fixed and paraffin-embedded (FFPE) blocks from the University Cancer Center Frankfurt (UCT) Biobank from 2017 to 2019. The tissue was used for either DNA isolation as detailed in the corresponding segment or generation of tissue microarrays (TMAs). Further information regarding this patient cohort is summarised in File S1 (EPIC-Cohort).

MtDNA copy number analyses were performed in 22 patients with *IDH*wt or *IDH*mut primary and recurrent gliomas. DNA was extracted from 48 FFPE tissue samples from 22 patients and RT-qPCR was performed. Additional clinical information regarding these patients is summarised in File S2 (MtDNA-Cohort).

For further analyses, we chose a historical cohort of 293 patients with glioma graded according to the 2007 4th edition of the World health Organization classification, including stratification with an antibody against *IDH1R132H*. All FFPE samples were processed as TMAs. All samples were collected as paraffin blocks from the UCT Biobank. Further data for this patient cohort and the analysed specimens are summarised in File S3 (Historical Glioma Cohort).

From all cohorts, we extracted a fourth cohort of 29 patients who received bevacizumab (Bev) during the course of their disease. All samples were collected as paraffin blocks before Bev treatment.

Further clinical data regarding this cohort are summarised in File S4 (Bev-Cohort).

The study was approved by the local ethics committee (GS 4/09, SNO-11-2017).

2.2 | IHC, microscopy, scoring and semi-automated digital quantification of immune cell infiltration

All TMA cores were punched from representative non-necrotic tumour areas. Three-micrometre thick sections of the TMAs were made with a microtome. The sections were placed on SuperFrost-Plus slides (Thermo Fisher Scientific, Waltham, MA, USA) and stored overnight in a 37°C incubator. IHC was performed using antibodies against the following antigens: semi-purified mitochondrial preparation anti-mitochondrial antibody (clone MTC02, dilution 1:100, Abcam, Cambridge, MA, USA), mitochondrial cytochrome c oxidase I (MT-CO1 (1:200 dilution, Cell Signaling Technologies, Danvers, MA, USA) and lactate dehydrogenase A (LDHA, 1:100 dilution, Cell Signaling Technologies). Throughout the text, MTC02 is used to denote the anti-mitochondrial antibody. Stained TMA slides were examined using a model BX41 microscope and images were taken with an attached DP72 camera (both from Olympus, Tokyo, Japan). For semi-quantitative evaluation, the H-Score was applied as described previously [35]. The relationships between the metabolic surrogate markers were investigated using quartile ratios of each tumour and the corresponding marker (1. quartile 0-25%, 2. quartile 25-50%, 3. quartile 50-75%, 4. quartile 75-100%).

Immune cell infiltration of the EPIC-Cohort was assessed histologically by IHC against CD8 (clone C8/144B, 1:100 dilution; DAKO, Glostrup, Denmark), CD68 (1:200 dilution;M0876, DAKO) and Iba1 (019-19741, 1:1000 dilution; Wako, Neuss, Germany). For semi-automated digital quantification of immune cell content, whole slide scanning of CD8, CD68 and Iba1 staining was performed using an Axio ScanZ.1 (Carl Zeiss Microscopy GmbH, Jena, Germany) with a 20× objective lens. Scanned images in the. czi file format were uploaded into HALO™ Next-Generation Image Analysis software (Version 3.0.311.287, Indica Labs, Albuquerque, NM, USA). Segmentation of TMA cores and exclusion of tumour necrosis, larger vessels and artefacts were performed using implemented software tools. Furthermore, the multiplex IHC module was employed to count total cells and positive cells for CD8, CD68 and Iba1.

2.3 | DNA isolation for mtDNA copy number analyses

Tissue specimens from FFPE samples were examined using haematoxylin and eosin staining to determine non-necrotic regions of tumour tissue. One or two cores 2 mm in diameter and 3 to 5-mm thick were punched out from the selected regions of the paraffin blocks. DNA was extracted using the Stratec Genomic DNA Kit (Stratec, Berlin, Germany) according to the manufacturer's protocols.

2.4 | Real-time quantitative PCR (RT-qPCR)

Isolated DNA was diluted to a concentration of 10 ng/µl. RT-qPCR was performed using SYBR Green Master Mix (Thermo Fisher Scientific) on a CFX96Real-Time PCR Detection System (BIO-RAD, Hercules, CA, USA). Beta-2 microglobulin primers were used as a nuclear DNA amount reference (forward: gctgggtagctctaaacaatgtattca; reverse: ccatgtactaacaaatgtctaaaatggt) and compared to two pairs of primers targeting the D-Loop of the mitochondrial DNA (mtDNA) genome (MtDLoop1: forward: gtgaaatcaatatcccgcacaagag; reverse: tatgaccctgaagtaggaaccaga; MtDLoop2: forward: caccagcctaaccagatttca; reverse: agtatgggagtgggaggg). Analyses were performed in triplicate. Cycle threshold (CT) values were determined. Relative mtDNA copy number was calculated using the following previously described formulae [36]: ΔCT = (nucDNA CT – mtDNA CT) and Relative mitochondrial DNA content =2 × 2ΔCT.

2.5 | EPIC DNA methylation analysis

DNA from 57 patient samples was isolated as described above. CpG sites illustrated in the text were analysed with the EPIC 850 K Array (Illumina, San Diego, CA, USA). After standardised DNA processing, bisulphite treatment and further processing and hybridisation were performed as recommended by the manufacturer and previously described [16]. The resulting data were processed using Illumina Genome Studio, JMP14 (SAS Institute, Cary, NC, USA) and Partek Genomic Suite software (Partek Incorporated, St. Louis, MO, USA). The chosen gene sets and CpG sites included for analyses are listed in Supplementary Information 5 + 6. Only CpG sites with a potential single nucleotide polymorphism with minor allele frequency (MAF) <0.01 (1%) were included in the analyses. Promoter-associated CpGs were chosen based on their provided information (regulatory feature group). Ten thousand CpGs with the highest average deviation were chosen for main clustering (File S6). Shared CpGs between the chosen gene set and the 10 000 most variable CpGs were investigated using the online tool provided by VIB/UGent Bioinformatics & Evolutionary Genomics http://bioinformatics.psb.ugent.be/webtools/Venn/. All patient samples were classified according to the previously described molecular classification [16].

2.6 | DNA methylation-based immune cell deconvolution

The deconvolution was performed using RnBeads 2.0, which includes the leukocytes unmethylation for purity (LUMP) algorithm. This algorithm estimates the immune cell content of tumours based on 44 non-methylated immune-specific CpG sites [37,38].

2.7 | Data visualisation and statistical analyses

All statistical analyses were performed using either JMP11/14 (SAS Institute) or R (R Core Team, 2019). Epigenomic and IHC data visualisation were performed with R utilising a ComplexHeatmap-package [39] to generate heat maps and hierarchical clustering, and JMP11/14. JMP add-in with the R-package Rtsne was used to generate t-distributed stochastic neighbour embedding (t-SNE) plots.

3 | RESULTS

3.1 | DNA methylation profiling defines distinct metabolic clusters of diffuse gliomas.

In the first approach, analysis of 57 patients in the EPIC-Cohort for the 10,000 most variable CpG sites revealed strong clustering into *IDH*mut and *IDH*wt tumours, as well as the strong association of clusters with established molecular subclasses (File S7). To determine the epigenetic regulation of cellular bioenergetics, we defined gene subsets based on their involvement in glycolysis and oxidative phosphorylation either directly (e.g. facilitation of specific reactions) or indirectly (e.g. initiation of transcription of the mitochondrial genome). For gene set information, please see File S5. Furthermore, we added nuclear-encoded genes involved in the electron transport chain, which resulted in 2542 investigated 'Metabol' CpG sites of these genes represented on the EPIC Array (Figure 1, File S6). Mitochondria-encoded genes and potential DNA methylation of these genes were not represented in the applied EPIC Array.

Hierarchical cluster analyses based on beta values of the corresponding CpG site as well as t-SNE analyses clearly differentiated tumours according to their *IDH* mutation status (Figure 1A,B). The results indicated a correlation of the methylation status of metabolism-associated genes with the *IDH* mutation status (Figure 1A,B). Although *IDH*mut gliomas displayed a CpG site hypermethylation phenotype as compared to *IDH*wt gliomas, this did not entirely refer to the investigated 'Metabol' CpG site gene cluster. In contrast, methylation profiles appeared similar to a certain extent. Only a small subset of CpG sites seemed to determine the different clusters. Interestingly, clustering can not only separate *IDH*mut from *IDH*wt tumours, but also suggests subclustering into known epigenetic subgroups [16,17].

Next, we assessed the most relevant shared CpGs between the groups of most variable CpGs and 'Metabol' CpGs. Only 17 CpG sites were shared from both the 'Metabol' CpG site cluster and from the 10,000 most variable CpGs in the EPIC-Cohort (see the Venn diagram presented in Figure 1C). The genes with the most represented shared CpGs were the glycolytic gene *PFKP*, encoding the enzyme phosphofructokinase and the *ATP5G2* gene, which encodes a subunit of the mitochondrial ATP synthase (Figure 1D). These 17 CpG sites were able to discriminate *IDH*mut from *IDH*wt tumours (File S7).

3.2 | LDHA promoter-associated CpGs are highly regulated in different glioma subtypes

LDHA is upregulated in *IDH*wt glioma as compared to *IDH*mut glioma [40]. Furthermore, a recent study reported the increased hypomethylation of *LDHA* promoters during malignant progression in *IDH*mut gliomas [41]. To further investigate potential functionally relevant methylation patterns in gliomas, we investigated only annotated promoter-associated CpGs of the group of shared CpGs (Figure 1D), including *LDHA* promoter-associated CpGs (Figure 2A). The analysis led to the investigation of 65 CpG sites in the EPIC-Cohort. The resulting clusters were again almost exclusively linked to the *IDH* mutation status of the samples. Many of these promoter-associated CpGs were hypomethylated. Only promoter-associated CpGs of *ATP5G2* and *LDHA* showed obvious differential methylation in the molecular subgroups (Figure 2A). Interestingly, *LDHA* promoter-associated CpG sites were hypermethylated in almost all *IDH*mut tumours, while some showed hypermethylation only in a subset of CpG sites. Interestingly, none of the 1p/19q co-deleted tumours showed a fully hypomethylated *LDHA* promoter, whereas some *IDH*mut astrocytomas and high-grade astrocytomas presented with *LDHA* promoter hypomethylation. All*IDH*wt gliomas showed a hypomethylated *LDHA* promoter. These collective observations implicated *LDHA* promoter-associated CpG site hypomethylation as a feature associated with glioma aggressiveness and potentially associated with malignant progression of high-grade *IDH*mut astrocytomas. The *ATP5G2* promoter-associated CpG site methylation patterns were not entirely associated with *IDH* mutation status. Nevertheless, *IDH* mutant tumours showed a hypermethylated phenotype, which was also observed in some *IDH*wt tumours (Figure 2A). In contrast, the promoter-associated CpGs of *NDUFV2A*, which encodes the NADH-ubiquinone oxidoreductase complex (complex I) of the mitochondrial respiratory chain, was unmethylated in any sample from the EPIC-Cohort, suggesting that these genes are essential for cellular energy homoeostasis.

To assess whether the epigenetic switch of *LDHA* promoter methylation and demethylation has direct effects on the protein level, we investigated LDHA expression via IHC (Figure 2B). LDHA expression at the immunohistochemical level was significantly correlated with *LDHA* promoter methylation status (Figure 2C,D). The findings directly linked epigenetic regulation to protein expression.

3.3 | Copy number of mtDNA is linked to IDH mutational status

The foregoing data showed that several promoters of genes that might be needed for cellular energy homoeostasis were not differentially methylated between *IDH*wt and *IDH*mut tumours, including NDUFV2. Thus, we were interested in determining whether the total mitochondrial biomass varied between these glioma subgroups. To gain insights into mitochondrial biomass, we used mtDNA copy number as a surrogate in our mtDNA-Cohort. The mtDNA copy number was higher

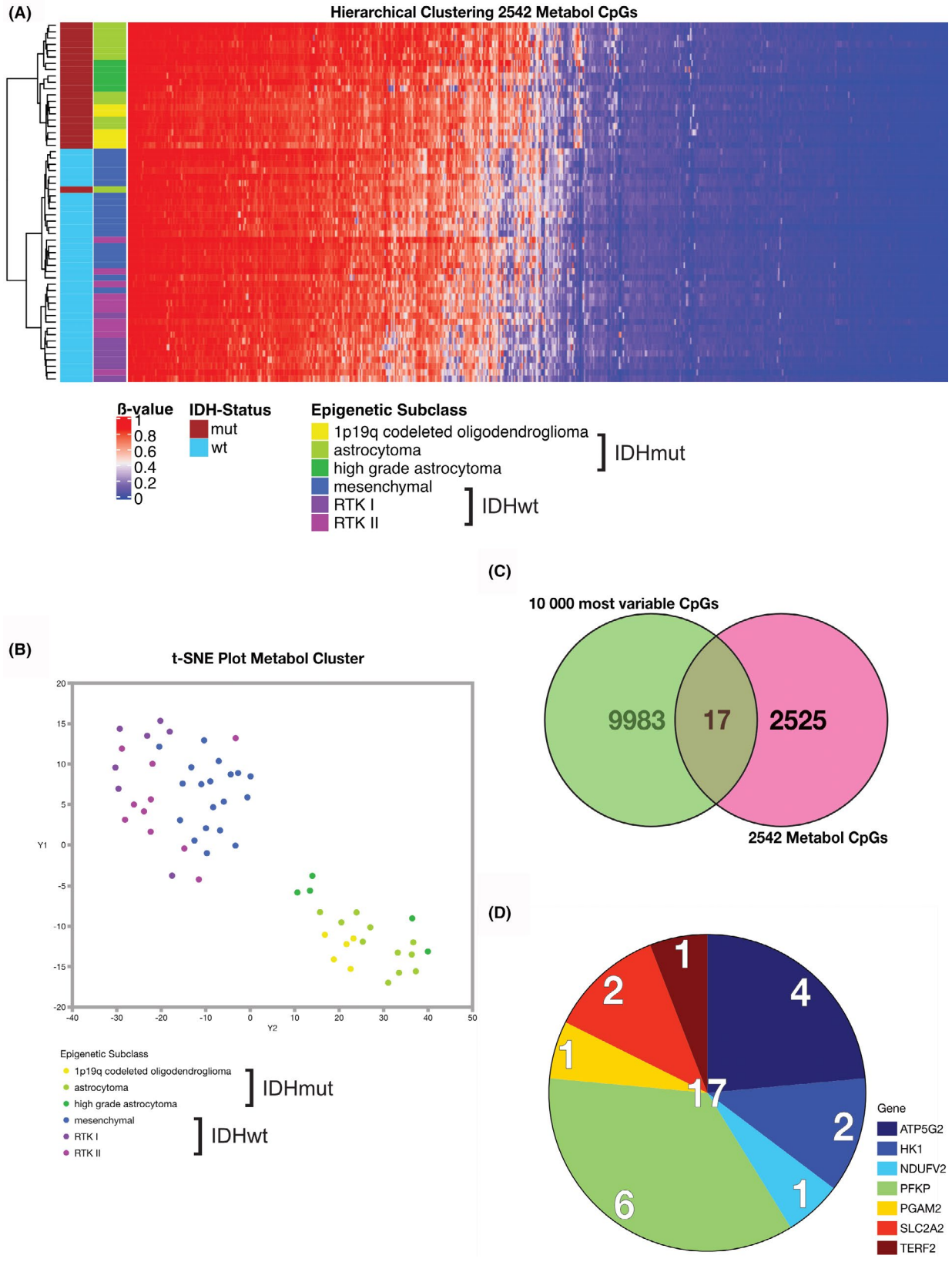

FIGURE 1 (A) Hierarchical clustering of 57 glioma patients (EPIC-Cohort) and 2542 CpG sites belonging to metabolic genes. (B) t-SNE plot of the same patients and 2542 CpG sites. (C) Venn diagram of 10,000 most variable CpG sites and 2542 metabolic CpG sites among the 57 glioma patients. Seventeen CpG sites were shared in both cohorts. (D) Gene symbols of genes corresponding to the shared 17 CpG sites. Number of CpG sites per gene are depicted in the pie chart

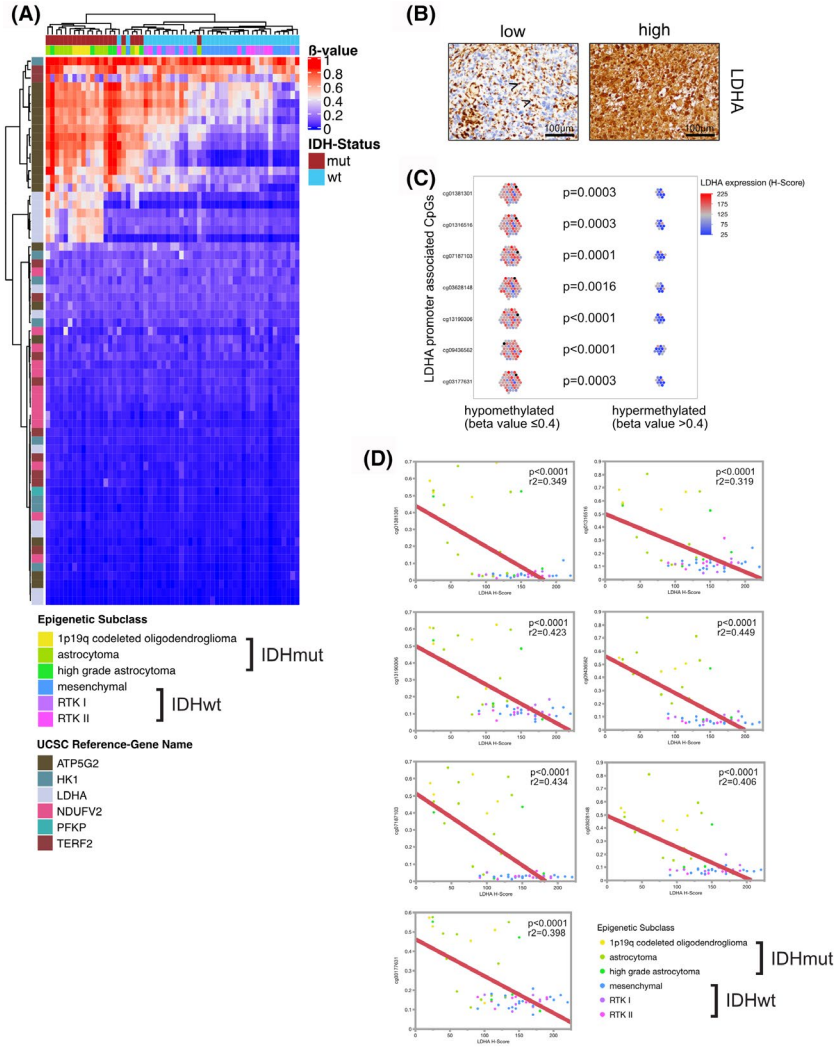

FIGURE 2 (A) Hierarchical clustering of 57 glioma patients (EPIC-Cohort) and 65 CpG sites of six metabolic genes (including *LDHA*) being annotated as promoter associated. Genes were chosen based on the results of shared CpGs (see Figure 1c). (B) LDHA protein expression in gliomas showing high and low expression. The left panel shows mostly negative tumour cells but positive microglia/macrophages (indicated by arrowheads). (C) Dichotomised comparison of *LDHA* promoter methylation status and protein expression. P-values of nonparametric Wilcoxon testing are depicted. (D) Correlation analyses of *LDHA* promoter-associated CpG sites (betavalues) and LDHA protein expression, assessed by H-Score

in *IDH*mut tumours than in *IDH*wt tumours (Figure 3A). Furthermore, when comparing primary with matched pair recurrent tumours, mtDNA copy number was not statistically significantly different, although some patients showed differences in mtDNA copy number between primary and recurrent tumours (Figure 3B). To extend these results to the proteomic level, we employed two immunohistochemical biomarkers. One was the antibody to MTC02, which recognises a 60-kDa non-glycosylated protein component of mitochondria. We used this as a surrogate for mitochondrial biomass. We also used MT-CO1, which is essential for oxidative phosphorylation as an integral part of the electron transport chain (Complex IV). MT-CO1 serves as a surrogate for mitochondrial respiratory capacity (Figure 3C).

Correlation of the relative expression of these proteins with mtDNA copy number revealed a positive correlation between mtDNA copy number and MTC02. No correlation was evident between mtDNA copy number and MT-CO1, or between MTC02 and MT-CO1 (Figure 3D). The findings implicated MTC02 as a useful surrogate biomarker for mitochondrial biomass but also suggested that pure mitochondrial biomass might not be directly linked to functionality. Finally, a higher relative mtDNA copy number was associated with better patient overall survival (Figure 3E).

3.4 | IHC of metabolic surrogate biomarkers reveals strong association with IDH mutation status and mesenchymal signature in IDHwt gliomas

Next, we were interested in further comparing our epigenetic findings of the EPIC-Cohort with protein expression of metabolic surrogate biomarkers of the mtDNA-Cohort. As metabolic surrogates,

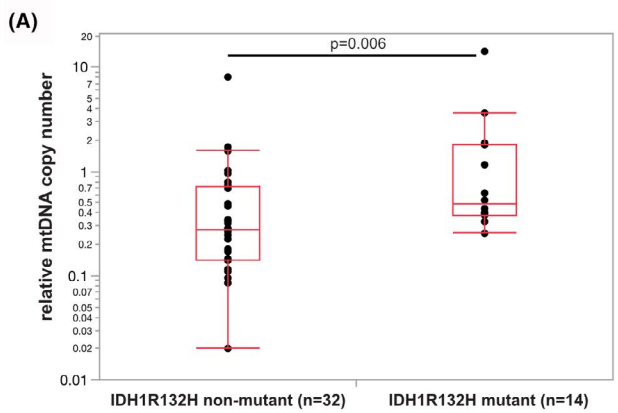

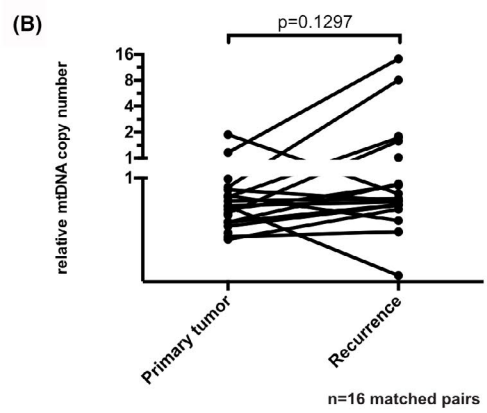

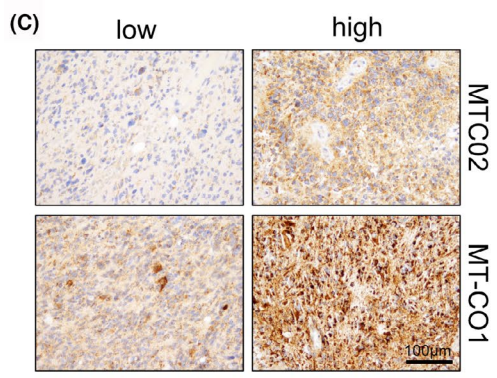

(D)

	relative mtDNA copy number	MTC02 (H-Score)	MT-CO1 (H-Score)
relative mtDNA copy number		r^2=0.123 p=0.0168	r^2=0.007 p=0.5785
MTC02 (H-Score)	r^2=0.123 p=0.0168		r^2=0.001 p=0.8468
MT-CO1 (H-Score)	r^2=0.007 p=0.5785	r^2=0.001 p=0.8468	

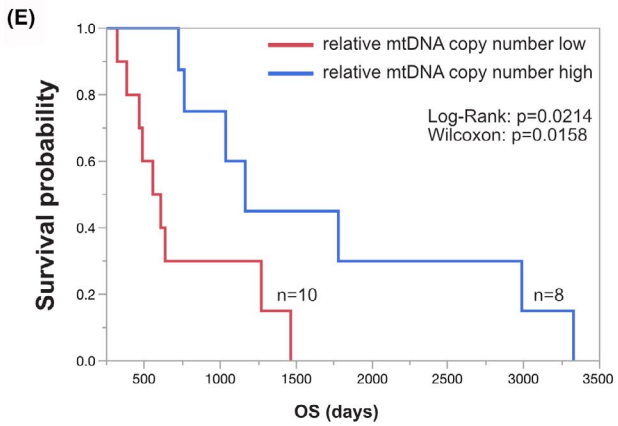

FIGURE 3 (A) Relative mtDNA copy number of *IDH*mut and *IDH*wt gliomas (mtDNA-Cohort). (B) Comparison of relative mtDNA copy number of primary tumours and corresponding recurrent tumours (p-values of nonparametric Wilcoxon tests are depicted in (A) and (B)). (C) MTC02 and MT-CO1 protein expression in gliomas showing high and low expression. (D) Correlation analyses of MTC02 and MT-CO1 protein expression as well as relative mtDNA copy number. (E) Kaplan–Meier survival chart of mtDNA-Cohort with regard to high or low-relative mtDNA copy number (dichotomised after median split)

we used the aforementioned targets of LDHA (glycolysis), MTC02 (mitochondrial biomass) and MT-CO1 (electron transport chain/oxidative phosphorylation).

In the first approach, we were interested in the expression of these metabolic surrogates in epigenetically defined gliomas. LDHA expression was significantly lower in *IDH*mut subclasses than in *IDH*wt glioma subclasses (Figure 4A). LDHA expression was not different within the epigenetic subclasses of *IDH*wt tumours. In contrast, MTC02 showed very low expression in the RTKII subclass of *IDH*wt gliomas. This class represents the classical GB molecular signature. MTC02 levels were significantly higher in mesenchymal *IDH*wt gliomas, *IDH*mut 1p/19q co-deleted oligodendrogliomas and *IDH*mut astrocytomas (Figure 4B). These observations indicated pronounced differences in mitochondrial biomass within the molecular subgroups of *IDH*wt GB. Mesenchymal GBs displayed the highest MT-CO1 levels among the *IDH*wt gliomas and in the whole EPIC-Cohort. Significant differences compared to RTKI (proneural) *IDH*wt gliomas and

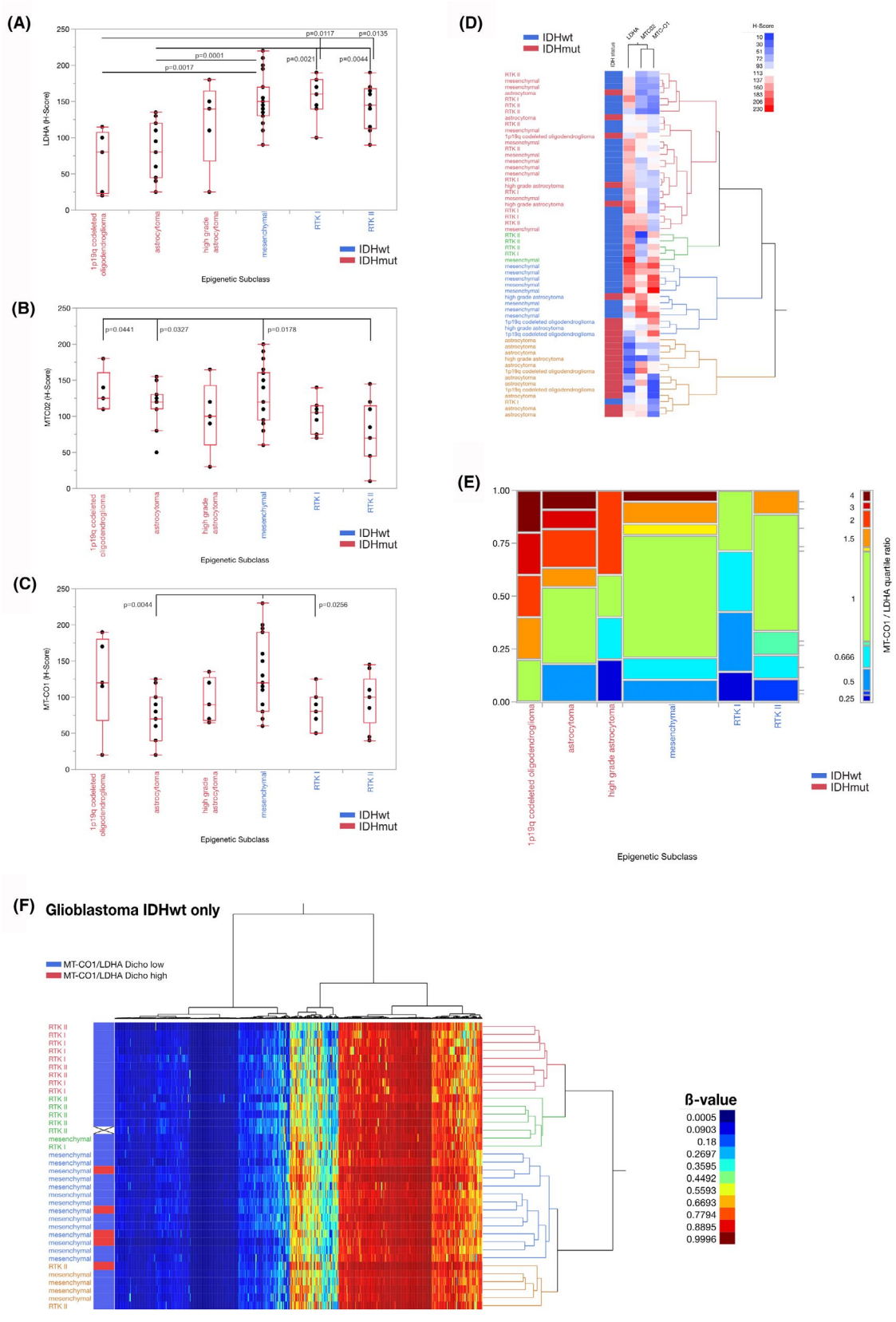

FIGURE 4 H-Scores of LDHA (A), MTC02 (B) and MT-CO1 (C) in the epigenetically characterised EPIC-Cohort (n = 56; in one case staining results were non-conclusive, thus this case was excluded from analyses). (D) Cluster analysis of EPIC-Cohort with regard to LDHA, MTC02 and MT-CO1 H-Score expression. (E) MT-CO1/LDHA quartile ratios of the EPIC-Cohort. (F) Cluster analysis of the 2542 CpG sites belonging to metabolic genes with special regard to epigenetic subtype of *IDH*wt gliomas and MT-CO1/LDHA quartile ratios (high versus low; (single case with missing IHC data is marked with 'X')

*IDH*mut astrocytomas (Figure 4C) suggested that *IDH*wt gliomas with a mesenchymal signature tend to be associated with a more oxidative phosphorylation phenotype.

We combined the expression profiles of the three metabolic surrogate markers to an IHC panel and performed hierarchical cluster analysis. Strong enrichment of oxidative phosphorylating tumours and glycolytic tumours was evident (Figure 4D).

To gain insights into whether the different glioma subclasses in our cohort favoured anaerobic glycolysis over oxidative phosphorylation, as described by the Warburg effect, we analysed LDHA expression in relation to MT-CO1 expression. We generated quartile ratios for each specimen and metabolic surrogate marker (Figure 4E). The quartile ratio showed higher values in the *IDH*mut subclasses than in the *IDH*wt subclasses. These results confirmed our epigenetic and genetic results of *LDHA* hypermethylation and higher mitochondrial respiratory capacity in *IDH*mut tumours.

To investigate whether this ratio was defined by an epigenetic signature of metabolic genes in *IDH*wt glioma subclasses, we performed hierarchical clustering based on the 2542 'Metabol' CpGs and annotated dichotomised MT-CO1/LDHA quartile ratios (high versus low; Figure 4F). Clustering revealed four subgroups linked to the *IDH*wt epigenetic subclasses. We observed five tumours with high MT-CO1/LDHA ratios. Interestingly, these tumours almost exclusively belonged to the mesenchymal subclass of gliomas.

3.5 | Immune cell content is associated with epigenetic subclass but not with MT-CO1/LDHA ratio

To evaluate the impact of immune cell composition on the detected signatures, we employed tumour deconvolution analyses based on the EPIC Array data (LUMP algorithm) as well as immune cell quantification using IHC and semi-automated analysis of CD8, CD68 and Iba1. Immune cell infiltration was highest in *IDH*wt compared to *IDH*mut specimens with the highest immune cell levels in the mesenchymal subclass (Figure 5A). The predominant immune cell type was microglia (Figure 5B). CD8-positive T-lymphocytes were scarce in the analysed specimen, with mean frequencies ranging from 0.08% in 1p/19q co-deleted oligodendroglioma to 0.39% in mesenchymal subtype glioblastomas (Figure 5B). Immune cell content detected by epigenetic deconvolution strongly correlated with immune cell content detected by IHC and semi-automated analyses (Figure 5C). From all analysed metabolic markers, only LDHA expression was associated with immune cell content (Figure 5D). We did not detect statistically significant differences in cell type-specific immune cell content between MT-CO1/LDHA high versus low tumours (Figure 5E).

3.6 | Metabolic surrogate biomarkers are associated with patient prognosis in a large population-based glioma cohort

To test whether our results are applicable in a routine histopathological setting of non-epigenetically classified gliomas, we performed IHC analyses of LDHA, MTC02 and MT-CO1 in a historical Glioma Cohort of 293 patients.

Hierarchical clustering of LDHA, MTC02 and MT-CO1 H-Scores led to four major clusters. Cluster 2 was mainly enriched for *IDH*mut tumours, although it was not an exclusive *IDH*mut cluster (Figure 6A,B). Clusters 1 and 4 mainly represented two distinct immunohistochemical subgroups of *IDH*wt GB with only single *IDH*mut gliomas in both groups. Cluster 4 was generally defined by high LDHA expression and lower MTC02 and MT-CO1 expression. Cluster 4 was exclusive to GB (either *IDH*mut or *IDH*wt) and anaplastic *IDH*mut astrocytomas. *IDH*mut oligodendrogliomas or *IDH*mut astrocytomas were not present in this cluster (Figure 6B). To investigate whether this immunohistochemical signature impacted patient survival, we performed Kaplan–Meier analyses of all clusters. Cluster 4 displayed significantly worse survival compared to all other clusters when including all glioma subgroups (Figure 6C). To exclude bias induced by *IDH* mutation status, we performed the same analyses focussing only on *IDH*wt GB. Survival was worse in Cluster 4 patients than in Cluster 1 patients (Figure 6D).

3.7 | MT-CO1/LDHA quartile ratio is a biomarker for therapy response in Bev-treated gliomas

Finally, we hypothesised that the distinct metabolic status of gliomas would lead to different responses to a metabolically effective treatment strategy, such as anti-angiogenic treatment with Bev. We investigated glioma patients who received Bev as third-line therapy after standard treatment. Interestingly, higher levels of MT-CO1 as a single biomarker and in relation to LDHA expression was associated with a significantly better progression-free and overall survival after Bev treatment (Figure 7). These findings were independent of *IDH* mutational status and MGMT promoter methylation status in a multivariate parametric survival analysis (effect likelihood ratio progression-free survival: *IDH1R132H* status $p = 0.2431$, MGMT promoter methylation status $p = 0.1090$, MT-CO1/LDHA ratio $p = 0.0286$; effect likelihood ratio overall survival: *IDH1R132H* status $p = 0.0621$, MGMT promoter methylation status $p = 0.1668$, MT-CO1/LDHA ratio $p = 0.0016$).

4 | DISCUSSION

Since 2008, the increased understanding of tumour biology of diffuse gliomas with the discovery of *IDH* mutations has included the definition of new subclasses of gliomas [7]. Basic and translational studies have investigated the role of mutant *IDH* and discovered that *IDH* mutations result in a DNA and histone hypermethylation phenotype [10–15]. DNA methylation analyses permit precise tumour classification [16]. However, there is still a lack of understanding of the relationship between epigenetic changes and metabolism.

The aim of our study was to characterise the metabolic differences in diffuse gliomas with a special focus on epigenetic (DNA methylation) and proteomic (metabolic panel IHC) alterations, as

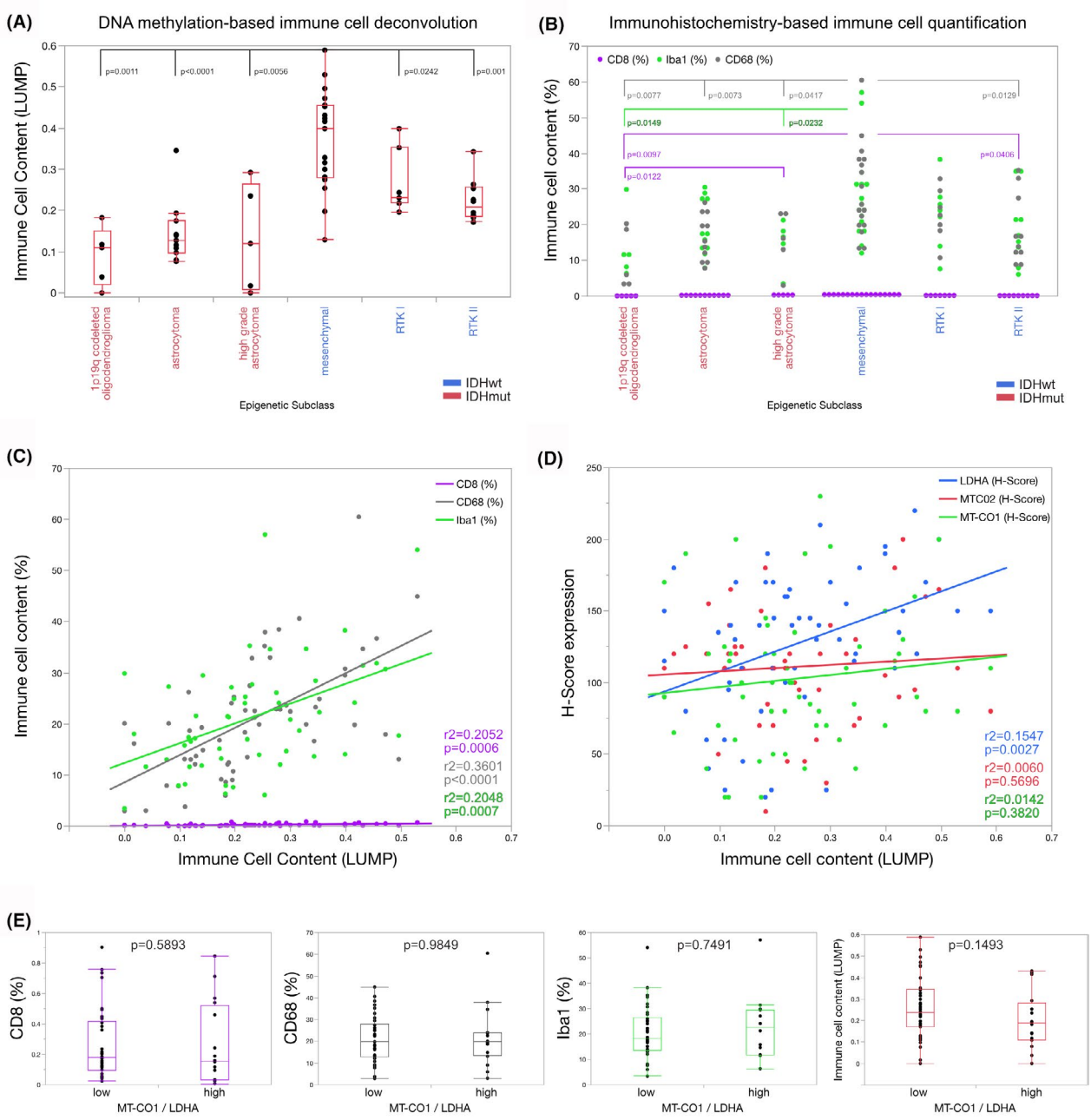

FIGURE 5 (A) DNA methylation-based immune cell deconvolution of the EPIC-Cohort. (B) Immunohistochemistry-based semi-automated immune cell quantification of the EPIC-Cohort. Correlation analyses of immune cell content (LUMP) and immune cell types (C) and metabolic markers (D). (E) Immune cell composition of MT-CO1/LDHA high versus low tumours. *p*-values of nonparametric Wilcoxon testing are depicted in (A), (B) and (E)

well as differences in mitochondrial biomass and genetics (metabolic panel IHC and D-Loop qPCR). We were able to confirm that *IDH*mut tumours showed a hypermethylated phenotype. The EPIC-Cohort displayed representative epigenomic alterations, which enabled us to further investigate metabolically relevant DNA methylation patterns. Hierarchical clustering of CpG sites belonging to metabolic genes was able to subclassify *IDH*mut and *IDH*wt tumours. Our analyses even showed a subgrouping of *IDH*wt gliomas in known epigenetic subclasses. In this context, the molecular subgroup of mesenchymal gliomas, which consists of GB with a mesenchymal signature, almost always contained a different metabolic signature as compared to the RTK I (proneural) and RTK II (classical) classes.

LDHA promoter-associated CpGs showed a hypermethylated phenotype in most *IDH*mut tumours, while all *IDH*wt gliomas were hypomethylated. To extrapolate the functional implications of these results, we showed that the methylation status of *LDHA* promoters was highly associated with LDHA expression at the protein level. This suggests epigenomic programming of *LDHA*, while general regulators of mitochondria were not differentially methylated in *IDH*mut

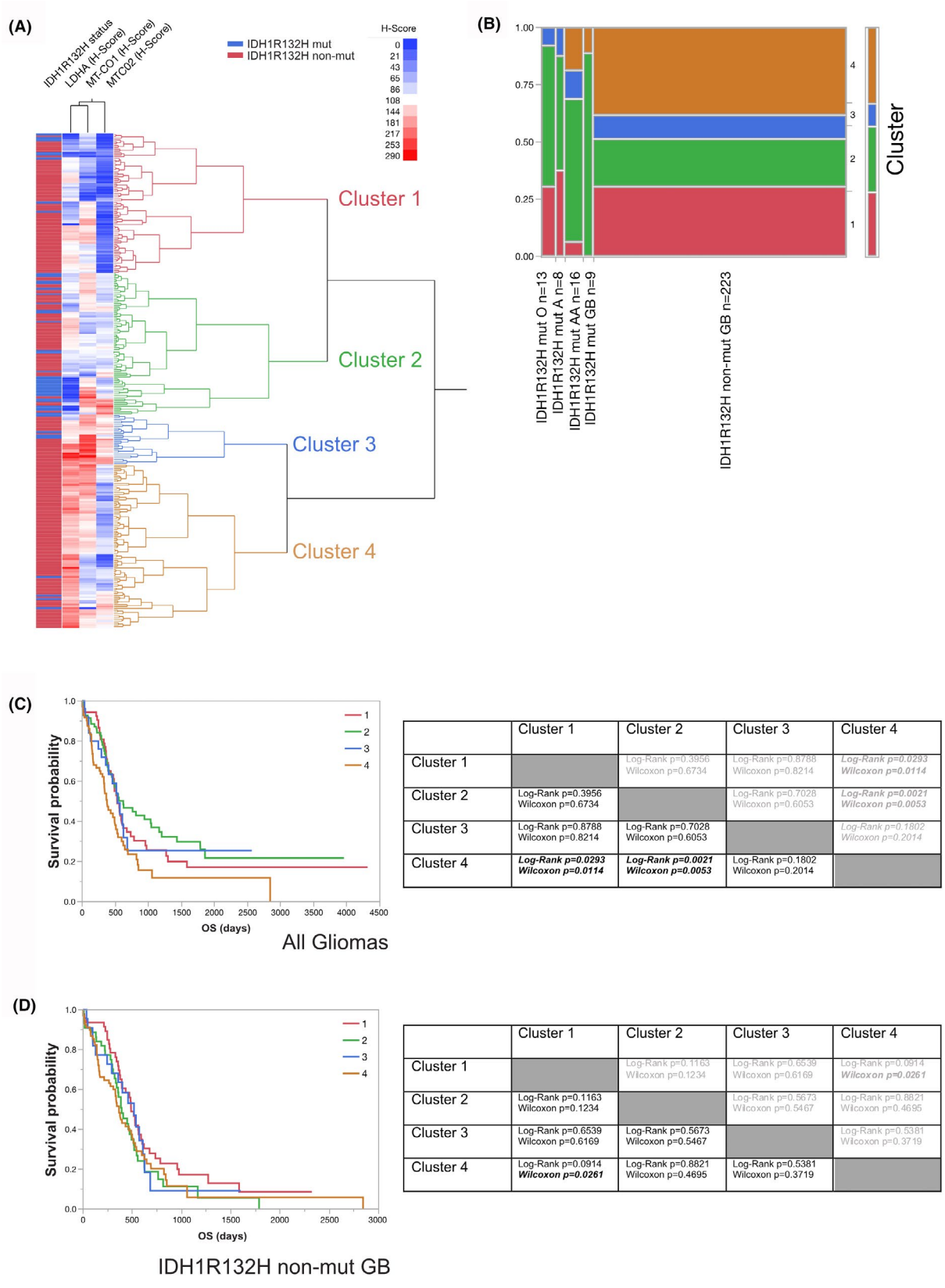

	Cluster 1	Cluster 2	Cluster 3	Cluster 4
Cluster 1		Log-Rank p=0.3956 Wilcoxon p=0.6734	Log-Rank p=0.8788 Wilcoxon p=0.8214	***Log-Rank p=0.0293*** ***Wilcoxon p=0.0114***
Cluster 2	Log-Rank p=0.3956 Wilcoxon p=0.6734		Log-Rank p=0.7028 Wilcoxon p=0.6053	***Log-Rank p=0.0021*** ***Wilcoxon p=0.0053***
Cluster 3	Log-Rank p=0.8788 Wilcoxon p=0.8214	Log-Rank p=0.7028 Wilcoxon p=0.6053		Log-Rank p=0.1802 Wilcoxon p=0.2014
Cluster 4	***Log-Rank p=0.0293*** ***Wilcoxon p=0.0114***	***Log-Rank p=0.0021*** ***Wilcoxon p=0.0053***	Log-Rank p=0.1802 Wilcoxon p=0.2014	

	Cluster 1	Cluster 2	Cluster 3	Cluster 4
Cluster 1		Log-Rank p=0.1163 Wilcoxon p=0.1234	Log-Rank p=0.6539 Wilcoxon p=0.6169	Log-Rank p=0.0914 ***Wilcoxon p=0.0261***
Cluster 2	Log-Rank p=0.1163 Wilcoxon p=0.1234		Log-Rank p=0.5673 Wilcoxon p=0.5467	Log-Rank p=0.8821 Wilcoxon p=0.4695
Cluster 3	Log-Rank p=0.6539 Wilcoxon p=0.6169	Log-Rank p=0.5673 Wilcoxon p=0.5467		Log-Rank p=0.5381 Wilcoxon p=0.3719
Cluster 4	Log-Rank p=0.0914 ***Wilcoxon p=0.0261***	Log-Rank p=0.8821 Wilcoxon p=0.4695	Log-Rank p=0.5381 Wilcoxon p=0.3719	

FIGURE 6 (A) Cluster analysis of LDHA, MTC02 and MT-CO1 H-Scores of the historical Glioma Cohort. Clusters 1-4 are highlighted by respective colours. (B) Contingency table showing distribution of Clusters 1-4 according to diagnosis. Panels (C) and (D) showing Kaplan–Meier charts according to Clusters 1-4. Panel (C) displays all gliomas, (D) only shows *IDH1R132H* non-mut glioblastomas. Tables on the right side illustrate the results of statistical analyses Clusters 1-4 versus Clusters 1-4. O: Oligodendroglioma, A: Astrocytoma, AA: Anaplastic Astrocytoma, GB: Glioblastoma

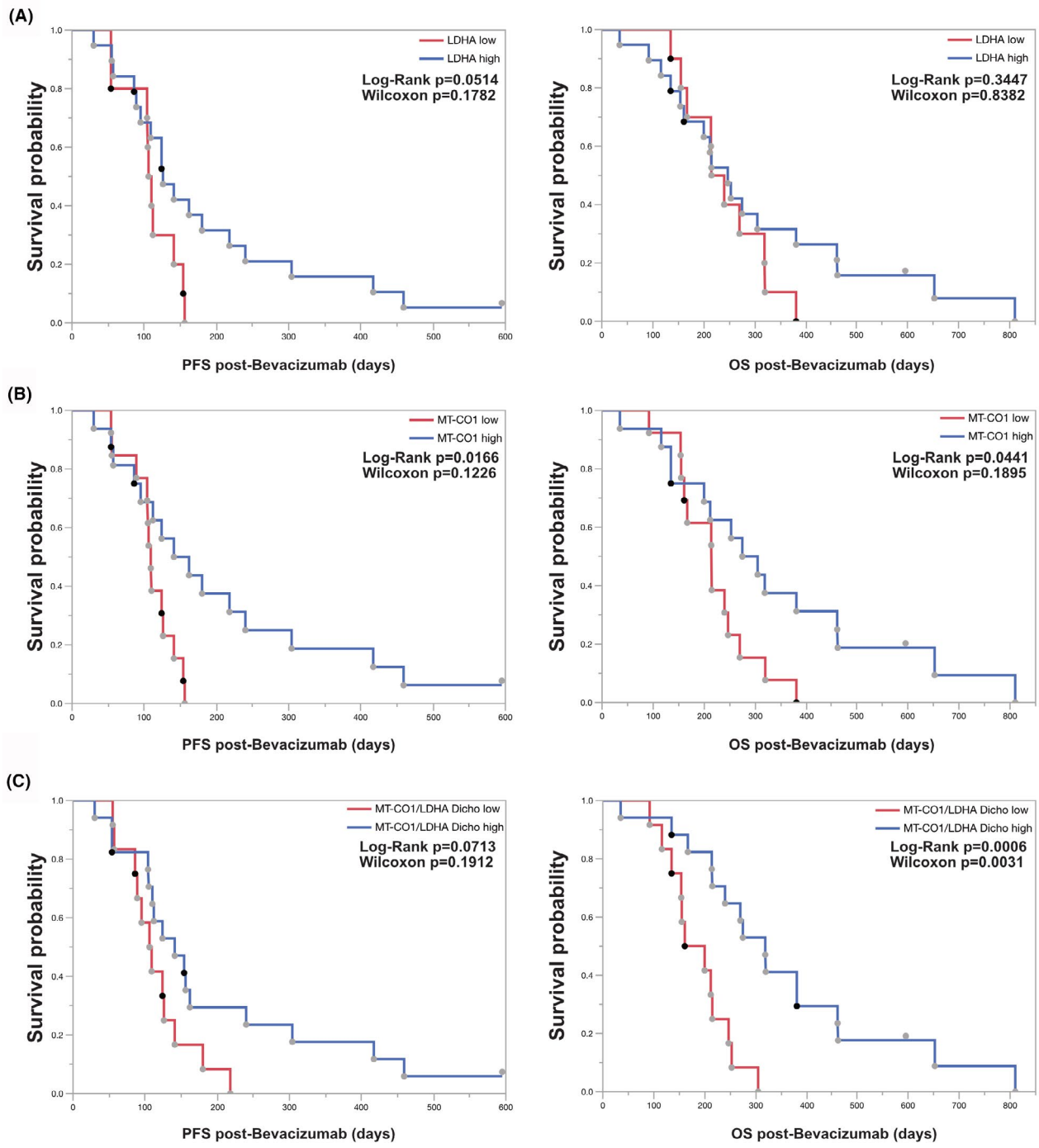

FIGURE 7 Kaplan–Meier survival analyses of the Bev-Cohort. Progression-free (PFS) and Overall survival (OS) stratified by (A) LDHA and (B) MT-CO1 expression as well as (C) MT-CO1/LDHA quartile ratio. High and low values were grouped after median split. Dots display single patients (black dots *IDH1R132H* mut, grey dots *IDH1R132H* non-mut tumours). Investigated tissue corresponds to last resection/biopsy before Bev treatment was initiated

versus *IDH*wt tumours. Our findings confirm the recent proposal of the DNA methylation-based reprogramming of glycolytic enzymes in *IDH*mut gliomas [41].

ATP5G2 was identified as one of the most extensively regulated genes at the DNA methylation level. *ATP5G2* encodes a subunit of the ATP Synthase complex V of the electron transport chain. We observed that most of the *ATP5G2* promoter-associated CpG-islands were hypermethylated in the *IDH*mut gliomas. Only a small subset of *IDH*wt samples also showed increased methylation, but in fewer CpG sites. *ATP5G2* has been previously described as being epigenetically regulated by DNA methylation in non-muscle invasive bladder cancer and renal cell carcinoma [42,43]. In these studies, *ATP5G2* was identified as a hypermethylated potential tumour suppressor gene that was increasingly inactivated

with malignancy. Interestingly, in the EPIC-Cohort in patients with *IDH*wt tumours promoter-associated CpG sites were mostly hypomethylated. Another study found that *ATP5G2* was upregulated in an ischaemic rat brain model. The authors described upregulated *ATP5G2* gene expression 24 h after artery occlusion [44], suggesting that *ATP5G2* gene expression is an early hypoxia/ischaemia response gene. The role of the expression of genes like *ATP5G2* in gliomas needs further investigation.

Cellular metabolism and the provision of bioenergetics are not only restricted to glycolysis. Thus, we were interested in whether the mitochondrial biomass varied between *IDH*mut and *IDH*wt tumours. We investigated our mtDNA-Cohort for mitochondrial DNA copy number variations. Interestingly, mitochondrial DNA copy number was higher in *IDH*mut tumours than in *IDH*wt tumours, suggesting a relatively increased mitochondrial signature in *IDH*mut tumours. Additionally, we showed that mitochondrial copy number correlated with a surrogate parameter of mitochondrial biomass (antibody MTC02) but not with protein expression of MT-CO1, a major contributor to oxidative phosphorylation. These findings underline that mitochondrial biomass should not be directly associated with mitochondrial functionality. In line with our findings, Navis and co-workers described higher amounts of mitochondria in an *IDH*mut glioma model [45]. Furthermore, in non-glial tumours, Farshidfar and co-workers identified an mRNA signature of *IDH*mut cholangiocarcinoma (CCA) enriched for genes involved in mitochondrial structure and function. The authors also described a higher mitochondrial DNA copy number in *IDH*mut CCA [46]. Our clinical data suggest that higher amounts of mitochondrial biomass are associated with a beneficial clinical course of diffuse gliomas. In this context, it is important to mention that mtDNA copy number did not significantly change between primary and recurrent tumours, indicating that, in contrast to the potential epigenetic adaptation of *LDHA* promoter hypomethylation, the mitochondrial biomass does not change throughout the clinical course. The reason for the elevated mitochondrial biomass in *IDH*mut as compared to *IDH*wt tumours remains speculative. In *Saccharomyces cerevisiae*, analogous to glioma-associated mutations of the $NADP^+$ isocitrate dehydrogenase, mutations resulted in increased levels of 2-hydroxyglutarate and extensive mtDNA loss, leading to a loss of respiratory capacity [47]. The gain of mitochondrial biomass is probably a compensatory mechanism of the cell to neutralise the toxic effects of 2-hydroxyglutarate. While it is plausible that the assumed reduced aerobic glycolysis in *IDH*mut gliomas could be associated with an increase in turnover in the citric acid cycle, a recent publication demonstrated the opposite [48].

We were able to further corroborate our findings at the protein level by applying a panel of metabolic biomarkers serving as surrogate parameters of mitochondrial biomass, glycolysis and oxidative phosphorylation. High LDHA expression indicative of a glycolytic bioenergetic status was clearly linked to *IDH*wt gliomas. Interestingly, when investigating the mitochondrial biomass and MT-CO1 as surrogate for oxidative phosphorylation in the EPIC-Cohort, mesenchymal *IDH*wt gliomas showed the highest levels for both. Not all mesenchymal *IDH*wt gliomas harboured this signature. Some did, indicating that mesenchymal *IDH*wt gliomas have the potential to have a mitochondrial signature.

When analysing DNA methylation signatures of tumour tissue, it should be considered that these signatures also reflect the non-tumour cell compartment. Cellular deconvolution revealed significant differences in immune cell infiltration in the distinct epigenetic glioma subclasses. In particular, mesenchymal GB showed high cellular heterogeneity with increased microglia/macrophage and lymphocyte infiltration, as previously reported [49,50]. Although there is a strong interaction between tumours and especially microglia, our data do not support the hypothesis that the metabolic signature is a pure immune cell signature. Our data indicate that key metabolic markers are not associated with immune cell content.

When we investigated metabolic aspects in our population-based historical Glioma Cohort, we detected two distinct subclasses of mainly *IDH*wt gliomas, while *IDH*mut gliomas were enriched in one cluster. Survival analyses revealed that the cluster of *IDH*wt tumours with high LDHA and low MT-CO1/MTC02 expression showed worse patient prognosis. This again emphasised that, in case of *IDH*wt status, a mitochondrial signature might be associated with better patient survival.

To further explore our hypothesis that metabolic surrogate biomarkers are prognosticators in gliomas, we analysed glioma tissue from patients treated with Bev. Strikingly, patients who showed a mitochondrial signature in their tumour tissue had significantly better overall survival following Bev treatment. These findings are consistent with experimental data demonstrating that glioma cells without functional mitochondria are resistant to Bev [51].Although this finding needs to be validated in larger cohorts of patients, these pilot data are compatible with the hypothesis that tumours with a mitochondrial signature are susceptible to anti-angiogenic therapy because they are less capable of adapting their metabolism to conditions of Bev-induced hypoxia.

In summary, the metabolism of *IDH*mut and *IDH*wt tumours differs substantially and relevant metabolic genes are regulated by DNA methylation. Furthermore, mitochondrial biomass is increased in *IDH*mut tumours and is stable during the clinical course. Importantly, even within *IDH*wt gliomas, a mitochondrial signature was associated with a better clinical outcome. At the epigenetic level, a mitochondrial signature was associated with the mesenchymal subclass in GB. Additionally, respiratory tumours may respond better to anti-angiogenic treatment than glycolytic tumours. The collective data indicate that for therapeutic regimens that either directly or indirectly affect tumour metabolism, the interrogation of multidimensional metabolic biomarkers is a promising strategy to define predictive signatures that can guide individualised treatment decisions.

ACKNOWLEDGEMENT

The authors thank Tatjana Starzetz and Maika Dunst for their technical support. Open access funding enabled and organized by Projekt DEAL.

CONFLICT OF INTEREST

JPS received grants from Merck and UCB as well as honoraria for lectures, travel, or advisory board participation from Abbvie, Bristol-Myers Squibb, Medac, Roche, Novocure and UCB. MWR has received research funding from the UCB. There are no conflict of interests specific to this manuscript.

AUTHOR CONTRIBUTIONS

YB and PNH designed the study; YB, KF, SB, BR, JZ, PB, PSZ, EI, MM and PNH performed the experiments; YB, BR, PB, PSZ, CS, MWR, OB, EH, MM and PNH involved in data acquisition and data collection; CS, KHP, EH and JPS provided material and clinical data; PNH involved in study supervision; All the authors involved in writing and editing the manuscript.

ETHICAL APPROVAL

The study was approved by the local ethics committee (GS 4/09, SNO-11-2017).

DATA AVAILABILITY STATEMENT

The data that support the findings of this study are available from the corresponding author upon reasonable request.

ORCID

Pia S. Zeiner https://orcid.org/0000-0001-6626-9211
Patrick N. Harter https://orcid.org/0000-0001-5530-6910

REFERENCES

1. Ostrom QT, Gittleman H, Liao P, et al. CBTRUS statistical report: Primary brain and other central nervous system tumours diagnosed in the United States in 2010–2014. *Neuro Oncol*. 2017; 19(5): v1–v88. https://doi.org/10.1093/neuonc/nox158
2. Ostrom QT, Bauchet L, Davis FG, et al. The epidemiology of glioma in adults: A state of the science review. *Neuro Oncol*. 2014; 16(7): 896-913. https://doi.org/10.1093/neuonc/nou087
3. Louis DN, Perry A, Reifenberger G, et al. World Health Organization classification of tumours of the central nervous system: a summary. *Acta Neuropathol*. 2016; 2016: https://doi.org/10.1007/s00401-016-1545-1
4. Yan H, Parsons DW, Jin G, et al. IDH1 and IDH2 mutations in gliomas. *N Engl J Med*. 2009; 360(8): 765-773. https://doi.org/10.1056/NEJMoa0808710
5. Louis DN, Perry A, Burger P, et al. International society of neuropathology-haarlem consensus guidelines for nervous system tumour classification and grading. *Brain Pathol*. 2014; 24(5): 429-435. https://doi.org/10.1111/bpa.12171
6. Ohgaki H, Kleihues P. The definition of primary and secondary glioblastoma. *Clin Cancer Res*. 2013; 19(4): 764-772. https://doi.org/10.1158/1078-0432.CCR-12-3002
7. Parsons DW, Jones S, Zhang X, et al. An integrated genomic analysis of human glioblastoma multiforme. *Science* 2008; (80-:). https://doi.org/10.1126/science.1164382
8. McLendon R, Friedman A, Bigner D, et al. Comprehensive genomic characterization defines human glioblastoma genes and core pathways. *Nature* 2008; 455(7216): 1061-1068. https://doi.org/10.1038/nature07385
9. Brennan CW, Verhaak RGW, McKenna A, et al. The somatic genomic landscape of glioblastoma. *Cell* 2013; 155(2): 462. https://doi.org/10.1016/j.cell.2013.09.034
10. Dang L, White DW, Gross S, et al. Cancer-associated IDH1 mutations produce 2-hydroxyglutarate. *Nature* 2009; 462(7274): 739-744. https://doi.org/10.1038/nature08617
11. Ward PS, Patel J, Wise DR, et al. The common feature of leukemia-associated IDH1 and IDH2 mutations is a neomorphic enzyme activity converting alpha-ketoglutarate to 2-hydroxyglutarate. *Cancer Cell* 2010; 17(3): 225-234. https://doi.org/10.1016/j.ccr.2010.01.020
12. Rohle D, Popovici-Muller J, Palaskas N, et al. An inhibitor of mutant IDH1 delays growth and promotes differentiation of glioma cells. *Science* 2013; 340(6132): 626-630. https://doi.org/10.1126/science.1236062
13. Venneti S, Thompson CB. Metabolic modulation of epigenetics in gliomas. *Brain Pathol*. 2013; 23(2): 217-221. https://doi.org/10.1111/bpa.12022
14. Noushmehr H, Weisenberger DJ, Diefes K, et al. Cancer Genome Atlas Research Network. Identification of a CpG island methylator phenotype that defines a distinct subgroup of glioma. *Cancer Cell* 2010; 17(5): 510-522. https://doi.org/10.1016/j.ccr.2010.03.017
15. Lu C, Ward PS, Kapoor GS, et al. IDH mutation impairs histone demethylation and results in a block to cell differentiation. *Nature* 2012; 483(7390): 474-478. https://doi.org/10.1038/nature10860
16. Capper D, Jones DTW, Sill M, et al. DNA methylation-based classification of central nervous system tumours. *Nature* 2018; 555(7697): 469-474. https://doi.org/10.1038/nature26000
17. Sturm D, Witt H, Hovestadt V, et al. Hotspot mutations in H3F3A and IDH1 define distinct epigenetic and biological subgroups of glioblastoma. *Cancer Cell* 2012; 22(4): 425-437. https://doi.org/10.1016/j.ccr.2012.08.024
18. Stupp R, Mason WP, Van Den Bent MJ, et al. Radiotherapy plus concomitant and adjuvant temozolomide for glioblastoma. *N Engl J Med*. 2005. https://doi.org/10.1056/NEJMoa043330
19. Wick W, Hartmann C, Engel C, et al. NOA-04 randomized phase III trial of sequential radiochemotherapy of anaplastic glioma with Procarbazine, Lomustine, and Vincristine or Temozolomide. *J Clin Oncol*. 2009; 27(35): 5874-5880. https://doi.org/10.1200/JCO.2009.23.6497
20. Bastien JIL, McNeill KA, Fine HA. Molecular characterizations of glioblastoma, targeted therapy, and clinical results to date. *Cancer* 2015; 121(4): 502-516. https://doi.org/10.1002/cncr.28968
21. Chen R, Cohen AL, Colman H. Targeted therapeutics in patients with high-grade gliomas: past, present, and future. *Curr Treat Options Oncol*. 2016; 17(8): https://doi.org/10.1007/s11864-016-0418-0
22. Touat M, Idbaih A, Sanson M, Ligon KL. Glioblastoma targeted therapy: updated approaches from recent biological insights. *Ann Oncol*. 2017; 28(7): 1457-1472. https://doi.org/10.1093/annonc/mdx106
23. Le Rhun E, Preusser M, Roth P, et al. Molecular targeted therapy of glioblastoma. *Cancer Treat Rev*. 2019; 80(September): 101896. https://doi.org/10.1016/j.ctrv.2019.101896
24. Maroon J, Seyfried T, Donohue J, Bost J. The role of metabolic therapy in treating glioblastoma multiforme. *SurgNeurol Int*. 2015. https://doi.org/10.4103/2152-7806.155259
25. Hanahan D, Weinberg RA. Hallmarks of cancer: The next generation. *Cell* 2011; 144(5): 646-674. https://doi.org/10.1016/j.cell.2011.02.013
26. Ward PS, Thompson CB. Metabolic reprogramming : A cancer hallmark even warburg did not anticipate. *Cancer Cell* 2012; 21(3): 297-308. https://doi.org/10.1016/j.ccr.2012.02.014
27. Zhou W, Mukherjee P, Kiebish MA, Markis WT, Mantis JG, Seyfried TN. The calorically restricted ketogenic diet, an effective alternative therapy for malignant brain cancer. *NutrMetab*. 2007. https://doi.org/10.1186/1743-7075-4-5
28. Rieger J, Bähr O, Maurer GD, et al. ERGO: A pilot study of ketogenic diet in recurrent glioblastoma. *Int J Oncol*. 2014; 45(6): 1843-1852. https://doi.org/10.3892/ijo.2014.2382

29. Scholz A, Harter PN, Cremer S, et al. Endothelial cell-derived angiopoietin-2 is a therapeutic target in treatment-naive and bevacizumab-resistant glioblastoma. *EMBO Mol Med*. 2016; 8(1): 39-57. https://doi.org/10.15252/emmm.201505505
30. Fack F, Espedal H, Keunen O, et al. Bevacizumab treatment induces metabolic adaptation toward anaerobic metabolism in glioblastomas. *Acta Neuropathol*. 2015; 129(1): 115-131. https://doi.org/10.1007/s00401-014-1352-5
31. Keunen O, Johansson M, Oudin A, et al. Anti-VEGF treatment reduces blood supply and increases tumour cell invasion in glioblastoma. *Proc Natl Acad Sci U S A*. 2011; 108(9): 3749–3754. https://doi.org/10.1073/pnas.1014480108
32. Warburg O, Wind F, Negelein E. The metabolism of tumours in the body. *J Gen Physiol*. 1927. https://doi.org/10.1085/jgp.8.6.519
33. Warburg O. On the origin of cancer cells. *Science (80-)* 1956. https://doi.org/10.1126/science.123.3191.309
34. Vander Heiden M, Cantley L, Thompson C. Understanding the warburg effect: the metabolic requirements of cell proliferation. *Science* 2009; 324(5930): 1029-1033. https://doi.org/10.1126/science.1160809
35. Zeiner PS, Zinke J, Kowalewski DJ, et al. CD74 regulates complexity of tumour cell HLA class II peptidome in brain metastasis and is a positive prognostic marker for patient survival. *Acta Neuropathol Commun*. 2018; 6(1): 18. https://doi.org/10.1186/s40478-018-0521-5
36. Rooney JP, Ryde IT, Sanders LH, et al. PCR based determination of mitochondrial DNA copy number in multiple species. *Methods Mol Biol*. 2015; 1241: 23-38. https://doi.org/10.1007/978-1-4939-1875-1_3
37. Müller F, Scherer M, Assenov Y, et al. RnBeads 2.0: comprehensive analysis of DNA methylation data. *Genome Biol*. 2019; 20(1):55. https://doi.org/10.1186/s13059-019-1664-9
38. Aran D, Sirota M, Butte AJ. Systematic pan-cancer analysis of tumour purity. *Nat Commun*. 2015; 4(6): 8971. https://doi.org/10.1038/ncomms9971
39. Gu Z, Eils R, Schlesner M. Complex heatmaps reveal patterns and correlations in multidimensional genomic data. *Bioinformatics* 2016; 32(18): 2847-2849. https://doi.org/10.1093/bioinformatics/btw313
40. Chesnelong C, Chaumeil MM, Blough MD, et al. Lactate dehydrogenase A silencing in IDH mutant gliomas. *Neuro Oncol*. 2013. pii: not243. doi: https://doi.org/10.1093/neuonc/not243
41. Victor RR, Malta TM, Seki T, et al. Metabolic Reprogramming Associated with Aggressiveness Occurs in the G-CIMP-High Molecular Subtypes of IDH1mut Lower Grade Gliomas. *Neuro Oncol*. 2019 Oct 30. pii: noz207. https://doi.org/10.1093/neuonc/noz207
42. Kitchen MO, Bryan RT, Emes RD, et al. Quantitative genome-wide methylation analysis of high-grade non-muscle invasive bladder cancer. *Epigenetics* 2016; 11(3): 237-246. https://doi.org/10.1080/15592294.2016.1154246
43. Morris MR, Ricketts CJ, Gentle D, et al. Genome-wide methylation analysis identifies epigenetically inactivated candidate tumour suppressor genes in renal cell carcinoma. *Oncogene* 2011; 30(12): 1390-1401. https://doi.org/10.1038/onc.2010.525
44. Chung JY, Yi JW, Kim SM, Lim YJ, Chung JH, Jo DJ. Changes in gene expression in the rat hippocampus after focal cerebral ischemia. *J Korean Neurosurg Soc*. 2011; 50(3): 173-178. https://doi.org/10.3340/jkns.2011.50.3.173
45. Navis AC, Niclou SP, Fack F, et al. Increased mitochondrial activity in a novel IDH1-R132H mutant human oligodendroglioma xenograft model: in situ detection of 2-HG and α-KG. *Acta Neuropathol Commun*. 2013; 29(1): 18. https://doi.org/10.1186/2051-5960-1-18
46. Farshidfar F, Zheng S, Gingras MC, et al. Integrative genomic analysis of cholangiocarcinoma identifies distinct IDH-mutant molecular profiles. *Cell Rep*. 2017;18(11):2780-2794. https://doi.org/10.1016/j.celrep.2017.02.033
47. Kingsbury JM, Shamaprasad N, Billmyre RB, Heitman J, Cardenas ME. Cancer-associated isocitrate dehydrogenase mutations induce mitochondrial DNA instability. *Hum Mol Genet*. 2016; 25(16): 3524-3538. https://doi.org/10.1093/hmg/ddw195
48. Biedermann J, Preussler M, Conde M, et al. Mutant IDH1 differently affects redox state and metabolism in glial cells of normal and tumour origin. *Cancers (Basel)*. 2019;11(12). pii: E2028. https://doi.org/10.3390/cancers11122028
49. Wang Q, Hu B, Hu X, et al. Tumour evolution of glioma intrinsic gene expression subtype associates with immunological changes in the microenvironment. *Cancer Cell* 2017; 32(1): 42–56.e6. https://doi.org/10.1016/j.ccell.2017.06.003
50. Kaffes I, Szulzewsky F, Chen Z, et al. Human Mesenchymal glioblastomas are characterized by an increased immune cell presence compared to Proneural and Classical tumours. *Oncoimmunology*. 2019; 8(11): e1655360. https://doi.org/10.1080/2162402X.2019.1655360
51. Eriksson JA, Wanka C, Burger MC, et al. Suppression of oxidative phosphorylation confers resistance against bevacizumab in experimental glioma. *J Neurochem*. 2018; 144(4): 421-430. https://doi.org/10.1111/jnc.14264

SUPPORTING INFORMATION

Additional supporting information may be found online in the Supporting Information section.

File S1: Clinical data of epic-Cohort (numbers in parentheses represent relative values). histopathology of idhwt and idhmut tumours is depicted at the bottom of the table.

File S2: Clinical data of mtDNA-Cohort (numbers in parentheses represent relative values).

File S3: Clinical data of historical Glioma Cohort (numbers in parentheses represent relative values).

File S4: Clinical data of Bev-Cohort (numbers in parentheses represent relative values).

File S5: Mitochondrial metabolism genes.

File S6: CpGs included in the analyses.

File S7. (a) Hierarchical clustering of 57 glioma patients and 10 000 most variable CpG sites. (b) t-SNE plot of the same patients and 10,000 most variable CpG sites. (c) Hierarchical clustering of 57 glioma patients and 17 CpG sites that were shared between the 10,000 most variable CpG sites and 2542 metabolic CpG sites.

How to cite this article: Braun Y, Filipski K, Bernatz S, et al. Linking epigenetic signature and metabolic phenotype in *IDH* mutant and *IDH* wildtype diffuse glioma. *Neuropathol Appl Neurobiol*. 2021;47:379–393. https://doi.org/10.1111/nan.12669